Aeroheating Thermal Analysis Methods for Aerobraking Mars Missions

Ruth M. Amundsen and John A. Dec
National Aeronautics and Space Administration
Langley Research Center
Hampton, VA 23681

Lt Benjamin E. George
United States Air Force
Kirtland Air Force Base
Albuquerque, NM 87111

ABSTRACT

Mars missions often employ aerobraking upon arrival at Mars as a low-mass method to gradually reduce the orbit period from a high-altitude, highly elliptical insertion orbit to the final science orbit. Two recent missions that made use of aerobraking were Mars Global Surveyor (MGS) and Mars Odyssey. Both spacecraft had solar arrays as the main aerobraking surface area. Aerobraking produces a high heat load on the solar arrays, which have a large surface area exposed to the airflow and relatively low mass. To accurately model the complex behavior during aerobraking, the thermal analysis must be tightly coupled to the flight mechanics, aerodynamics, and atmospheric modeling efforts being performed during operations. To properly represent the temperatures prior to and during the drag pass, the model must include the orbital solar and planetary heat fluxes. The correlation of the thermal model to flight data allows a validation of the modeling process, as well as information on what processes dominate the thermal behavior. This paper describes the thermal modeling method that was developed for this purpose, as well as correlation for two flight missions, and a discussion of improvements to the methodology.

INTRODUCTION

Two recent missions to Mars have used aerobraking at Mars as a method for decreasing required fuel mass: Mars Global Surveyor (MGS) and Mars Odyssey. Aerobraking is the process of skimming the spacecraft through the planetary atmosphere at periapsis, decreasing its speed and thus lowering apoapsis. This method saves substantially on the amount of fuel required to achieve the science orbit. The solar panels constitute the main drag on the spacecraft, and as low-mass “wings” they bear the brunt of aeroheating. The duration of aerobraking is often critical, due to high mission costs during that period, and because the duration of aerobraking affects the final science orbit.

The Mars Global Surveyor spacecraft launched in November of 1996 and arrived at Mars in September 1997. The initial orbit was highly elliptical, with an apoapsis of 54,026 km and a 45-hour period. Aerobraking was used to slow the spacecraft and decrease the orbit altitude to allow insertion into a final science orbit. The aerobraking effort was originally planned to take four months to bring the orbit apoapsis to 450 km. Early in the aerobraking, aerodynamic pressure caused one of Surveyor's two solar panels to bend backward slightly. The panel in question had been damaged shortly after launch. This event led to a pause in aerobraking and eventually a more conservative approach toward aerobraking, to put less stress on the damaged solar panel. Because of the discovery of the damaged solar panel which led to the mid-mission change in MGS aerobraking operations, only the first 15 passes were done in the original flight corridor at relatively high atmospheric densities with a comparatively high aeroheating environment. At the start of the aerobraking phase of the mission, the mission plan was to progressively lower the aerobraking altitude due to uncertainties in the density of the Mars atmosphere. Since correlation of the thermal model to high aeroheating environments was desired, pass 15, with the highest heating experienced, was the first one considered for correlation.

The Mars Odyssey mission was to use a similar mission plan as MGS, with solar arrays bearing the brunt of aerobraking. Thus it was important to fully understand the MGS mission performance. In particular, it was important to determine the thermal behavior of the solar arrays, since they were the limiting factor in aerobraking. If more aggressive aerobraking could be used (i.e., deeper cuts into the atmosphere on each pass), it would bring down the total time and cost for the Odyssey mission, as well as improving the ability to control the final science orbit. MGS flight data was used to correlate a thermal model of the solar arrays, to ensure that the behavior during aerobraking was fully quantified. Then, this information was used in the thermal analysis of Odyssey’s aerobraking which ultimately affected mission planning.

The Mars Odyssey spacecraft was launched on a Delta II launch vehicle from Cape Canaveral Air Force Station on April 7th 2001. On October 23rd 2001, the spacecraft performed a propulsive maneuver to insert itself into an 18.5-hour elliptic orbit around Mars. To achieve the 2-hour, 400km circular, sun-synchronous mapping orbit, Odyssey used the multipass aerobraking technique. The Magellan spacecraft (at Venus) was the first three-axis stabilized spacecraft to perform this type of multipass aerobraking.[1] To control periapsis altitude, Magellan planned on using thermocouple data to signal the need to perform a periapsis raise maneuver, which would raise the periapsis altitude, lower the maximum atmospheric density experienced, and thus lower the aerodynamic heating on the spacecraft and solar arrays. In the literature, it was noted that Magellan experienced at least 5 thermocouple failures prior to the start of aerobraking.[2] It is unclear from the available literature if any of these thermocouples were located on the solar arrays and were to be used during operations. It is also unclear whether or not there were any thermal models developed and used during the Magellan aerobraking process to make up for the inoperable thermocouples, but there are references to heat rate and surface temperature calculations being performed using a direct simulation Monte Carlo particle method.[3,4] In any event it is clear that in the early 1990's the limitations of computers would have prohibited the use of a detailed enough finite element or finite difference model that could have been run in a timely enough fashion to be used during operations. Mars Odyssey was the first multipass aerobraking mission to make use of detailed 3-dimensional finite element thermal model during operations to predict the temperatures for future orbits and reconstruct the solar panel temperatures for past orbits. This model, used in addition to a 1-dimensional model, provided detailed, 3-dimensional temperature profiles of the solar array, transient plots of maximum material temperatures, and transient plots of thermocouple temperatures.

SOLAR ARRAY DESCRIPTION

The function of the spacecraft solar arrays on both MGS and Mars Odyssey was two-fold. The primary function was to provide a stable power source for the spacecraft and scientific instruments during all phases of the mission. Second, during each drag pass of aerobraking, the solar arrays provided a large surface area on which the aerodynamic forces could act. For example, the Odyssey spacecraft began aerobraking by slicing through the Martian atmosphere at a relative velocity of about 4.57 km/s. Despite low atmospheric densities of about 80 kg/km^3, these high velocities produce significant aerodynamic heating on the solar array and spacecraft. Careful design and construction of the solar array allows it to withstand this aerodynamic heating.

The solar arrays on both spacecraft utilized a very similar layered construction of low density materials. Each panel consists of five layers; the first three make up the structural components and provide the structural integrity during launch and throughout aerobraking. The solar array structure is a sandwich construction with a 0.19 mm facesheet of M55J graphite composite, an aluminum honeycomb core (25 mm for MGS, 19.05mm for Odyssey), and another 0.19 mm M55J composite facesheet. The next layer is a 0.051mm Kapton sheet that is co-cured to the M55J graphite beneath it. Last is the solar cell layer, which consisted of the following, from the outside in: 0.152 mm cover glass, a layer of DC93500 adhesive, the solar cells themselves, a metal backing to the solar cells, and a layer of CV2568 adhesive that held the cells down to the Kapton sheet. On MGS, the solar cells were silicon on the outboard section of the array, and gallium arsenide (GaAs) on the inboard section, 0.19 mm thick. On Odyssey, all cells were GaAs. Figure 1 shows a cross-sectional view of the solar array at a representative location. On both arrays, certain sections of the standard 1.0 lb/ft^3 aluminum honeycomb core were replaced with a higher density core of the same thickness. Also, to reinforce at hard points, a thicker facesheet was used in some locations.

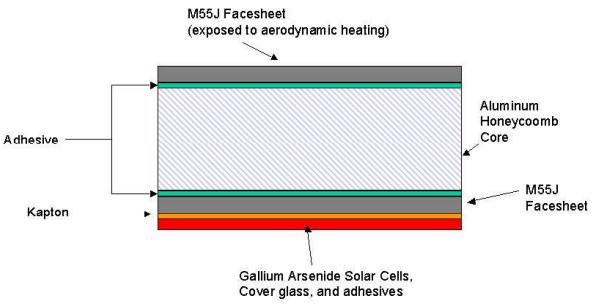

Figure 1. Cross-section of solar array (not to scale).

The MGS system is shown in Figure 2, and the Odyssey system in Figure 3. On MGS, the two panels are mounted on gimbals extending from the spacecraft. Since the extent of damage to the solar array on the -Y side of the space-

craft was unknown, only the +Y array was modeled and compared to flight data. The thermocouple locations are shown in Figure 4. On Odyssey, the panels are commonly referred to as the +X, -X, and mid panels. The +X and –X panels are mirror images of each other, while the mid panel has a unique geometry. Figure 5 shows a 3-dimensional geometric representation of the solar array as well as the five thermocouple locations. There is one thermocouple on the mid panel on the solar cell side of the array. The +X and – X panels each have one thermocouple on the solar cell side and one on the "hot" facesheet side. On the engineering drawings[5], the thermocouples are designated T1, T2, T3, T4, and T5.

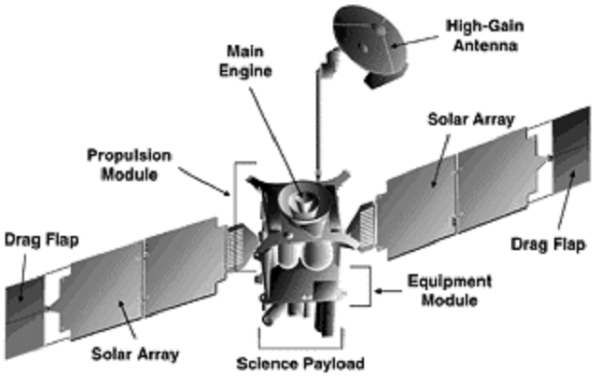

Figure 2. MGS spacecraft and solar arrays (*Courtesy JPL*).

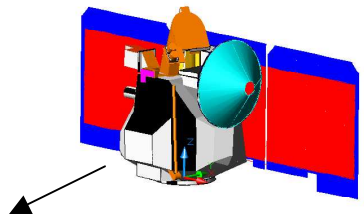

Figure 3. Mars Odyssey (Thermal Desktop model in the aerobrake configuration).

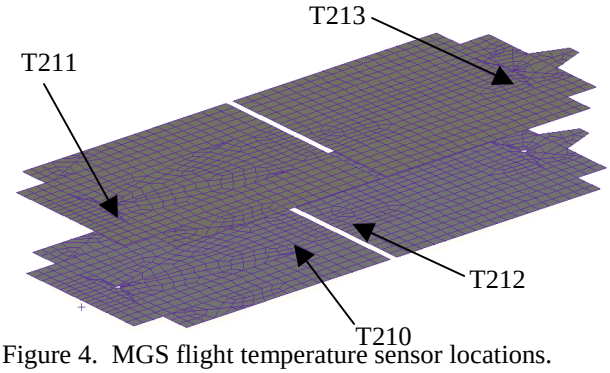

Figure 4. MGS flight temperature sensor locations.

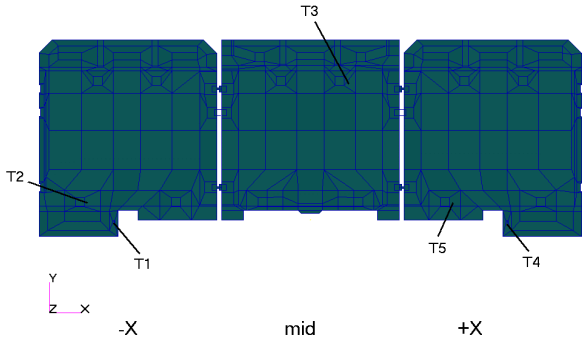

Figure 5. Mars Odyssey solar array and flight temperature sensor locations.

The MGS array had some white paint added at the edges to pre-cool regions of the array expected to receive the highest aerodynamic heating, and also had Kapton sheets layered on the corners to provide additional thermal mass to mitigate heating. To protect the Odyssey array from aerodynamic heating, a 0.072mm thick layer of multilayer insulation (MLI) was placed on the facesheet exposed to the aerodynamic heating and around the edges of the M55J graphite facesheet. The bulk of the MLI was on the facesheet surface, and a small portion wrapped around the edges and terminated on the solar cell side.

THERMAL MODEL DEVELOPMENT

The thermal methods have been described in detail elsewhere[6], but the basic methodology will be presented here. The thermal analysis of the solar array had three main components: the view factor and orbital heating analysis, the aerodynamic heating analysis, and the computation of solar array temperatures. The calculations were performed in two flight regimes. One regime was the vacuum phase where the spacecraft was in orbit around Mars, but out of the atmosphere. The thermal environment in this phase was dominated by the solar and planetary heating with negligible aerodynamic heating. The second regime was the aerobraking phase, or drag pass, where the spacecraft made its excursion into the atmosphere. The thermal environment in this phase was dominated by the aerodynamic heating with aerodynamic heating being roughly 60 times greater than the orbital heating. Temperatures were calculated for both flight regimes. Accurate calculation of the solar/planetary flux during flight, as well as aerodynamic heating during drag passes, requires that the thermal analysis be tightly coupled to the flight mechanics, aerodynamics, and atmospheric analysis. The orbital heating and view factor analysis, or radiation model, was developed using Thermal Desktop, a commercially available software package[7]. The radiation model was developed using engineering drawings of the spacecraft and solar array.[5] For Odyssey, view factor and heat rate calculations were performed for several different solar array configurations and spacecraft orientations. First, calculations were made with the spacecraft and solar array in its vacuum phase configuration; the spacecraft oriented with its high gain antenna pointed towards Earth and the solar array normal to the sun. In transitioning to the aerobrake configuration, both heat rates and view factors to space for the solar array were calculated as the solar array articulated to its stowed position. As the spacecraft slewed to the aerobraking configuration, the solar array's view factors to space did not change, so view factors did not have to be recalculated for that maneuver.

For the detailed thermal solution, a full thermal model was developed for the solar array only. For both missions, the solar arrays were mounted on gimbals with a low thermal conductance to the rest of the spacecraft, which minimized the conductive effect of the spacecraft on the array. The view factors to the spacecraft as well as solar and planetary fluxes from the radiation model were applied to the solar array model. This method allowed much more detail to be captured in the solar array thermal model without sacrificing solution time by having to include spacecraft elements in that model.

Radiation models

The radiation models of the spacecraft and solar arrays were developed in Thermal Desktop. The MGS model is shown in Figure 6 (arrows are used to indicate view angles to planet and Sun). The Odyssey radiation model is shown in Figure 7. The radiation models included all variations of optical properties, and were used to calculate viewfactors to space and orbital heat fluxes (solar and Martian).

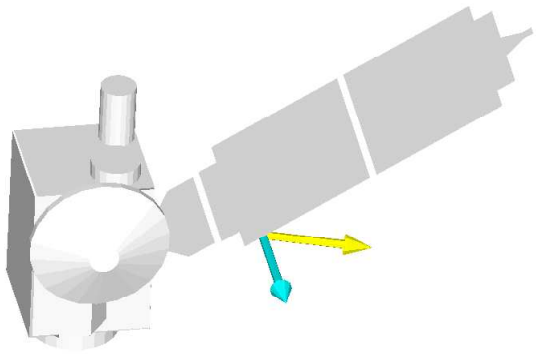

Figure 6. Radiation model in Thermal Desktop of MGS spacecraft/solar array.

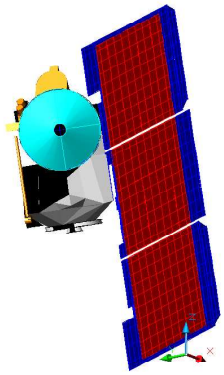

Figure 7. Thermal Desktop model of Mars Odyssey in the vacuum phase configuration (view from Earth).

Heating Model

The aerodynamic heating analysis consisted of calculating the atmospheric density, the spacecraft velocity relative to the atmosphere, and the heating coefficient for points spatially across the array. Using this information, the incident aerodynamic heating was calculated using equation 1,

$$Q_i = \frac{1}{2} \cdot \rho \cdot V^3 \cdot C_H \tag{1}$$

where ρ is the atmospheric density, V is the relative velocity, and C_H is the heat transfer coefficient. This calculation was made at 5 second intervals throughout the aerobraking pass to give a transient representation of aerodynamic heating. The flight mechanics team reconstructed the aerobraking pass and provided the relative velocity. The heating coefficients were calculated using a Direct Simulation Monte Carlo (DSMC) particle method. The density was calculated using acceleration readings from the flight accelerometer. The correlation of the atmospheric density to the accelerometers was made using DSMC which modeled the interaction of atmospheric particles with the entire spacecraft. The relation between the density and the acceleration is captured in equation 2,

$$ma = \frac{1}{2} c_d \rho V^2 \tag{2}$$

where m is the known mass of the spacecraft, a is the acceleration due to atmospheric drag, c_d is the drag coefficient determined using DSMC, ρ is the atmospheric density, and V is the velocity relative to the atmosphere. Using the density and the relative atmospheric velocity, the heating coefficients were calculated. Due to the long run times needed to perform the DSMC computations, an aerothermodynamic database was developed prior to aerobraking. Then for each time step, the density was calculated by interpolating the accelerometer data, and the heating coefficients across the array were calculated by interpolating between density and relative velocity. The interpolation error on the heating coefficients was calculated to be about 2%, which was within the accuracy of the DSMC calculations. The heat transfer coefficients ranged from a peak value of 0.90 to a low value of 0, and included the surface accommodation coefficient. The model also accounts for reflected heat, which was approximated empirically, and is a function of the incident heat flux and surface temperature. For MGS, the empirical equation is shown in (3) and (4), and for Odyssey it was as shown in (5).

$$C_{H,net} = C_{H,i} - \left[0.015 + 0.06 * (1 - C_{H,i})\right] * \left(T_{wall} / 300\right) \tag{3}$$

where the coefficients C_H are defined as:

$$C_H = q \Big/ \left(\tfrac{1}{2} \rho V^3\right) \tag{4}$$

$$Q_{ref} = \tfrac{1}{2}\rho V^3 \left[0.015 + 0.1\left(1 - \frac{Q_i}{\tfrac{1}{2}\rho V^3} \right) \right] \cdot \left(\frac{T_{wall}}{300} \right) \tag{5}$$

where T_{wall} is the surface temperature of the solar array. These calculations provided an accurate representation of the aerodynamic heating as well as reflected heating that was a function of time as well as position on the solar array.

Thermal Model

The full 3D thermal models for these missions were created in MSC/PATRAN[8]. This was done for two reasons. One was that existing FORTRAN code would allow simple inclusion of the aeroheating fluxes in PATRAN. The other was that the structural analysis of thermal stresses would be easily accomplished using existing methods. Normally, it is not more efficient to develop two models. However, in this case time constraints drove the use of existing, easily adapted methods. The duplicate model in Thermal Desktop was necessary since orbital capabilities do not exist within MSC/PATRAN.

The solar arrays were modeled in PATRAN as five distinct layers, as shown earlier in Figure 1. Each layer was modeled with plate elements, except for the aluminum core, which was modeled with solid elements. The layers were spaced apart, so that they could be connected via a contact conductance. This value could be varied to account for the adhesives used between the layers. Also, it accounted for the reduced contact area between the facesheets and honeycomb core. The solar cells were mounted over more than 90% of the surface on one side. Since the thermocouples that were used to correlate were in locations where coverage by solar cells is complete, it was decided to approximate the solar cell coverage as 100% to simplify modeling. The solar cell layer properties were calculated as a weighted average of the solar cells, cover glass, metal backing and adhesives. The wiring for the solar cells on each section was added to this layer as a smeared mass. During the drag passes the solar cell side was oriented away from the direction of flight, so that the bare graphite side, often referred to as the “hot” side, received the aerodynamic heating. The finite element mesh on the facesheets was customized to take the thermal sensor locations into account.

The models were highly detailed and included the variations in the aluminum honeycomb core density, the varying thickness of M55J composite doublers, and varied optical properties. An example of the varying thickness facesheet on MGS is shown in Figure 8. The titanium hinges and dampers that physically connect the solar panels were included in the models. For all materials, properties were included as functions of temperature; for the aluminum honeycomb core and M55J facesheets, orthotropic material properties were included. The spacecraft thermocouples were modeled as bar elements which had mass and were thermally connected via a contact resistance. Overall, each PATRAN thermal model was a physically accurate 3D representation of the solar array. The mass of each overall model was verified by a comparison with the as-built mass from flight assembly records. For MGS, the as-built mass of only the modeled portion was roughly 26 kg, while the mass of the total thermal model was 23 kg, for an error of 11%. Some inaccuracy in this model was tolerable since it was a post-flight model, not used for operations. For Odyssey, the as-built mass of the solar array was 32.3 kg, and the mass of the PATRAN thermal model was 33.4 kg, a difference of only 3.4%.

Boundary Conditions

Boundary conditions included contact conductance between layers, convection, radiation, aeroheating, and solar and planetary fluxes. The contact between layers was calculated as the effective conductance due to thickness of the materials themselves as well as the adhesive thickness.

The radiation boundary conditions included both internal and external radiation. Radiation through the aluminum core, from one facesheet to another, was applied. The view factors from the Thermal Desktop spacecraft model were applied as fields in the appropriate regions, by mapping the viewfactors into the PATRAN model, as shown in Figure 9 for MGS and Figure 10 for Odyssey. View factors to both space and the spacecraft were included. Space temperature was fixed at 3 K during the exo-atmospheric portion of the analysis, and then was allowed to vary to simulate the Martian atmosphere/space combination during the drag pass.

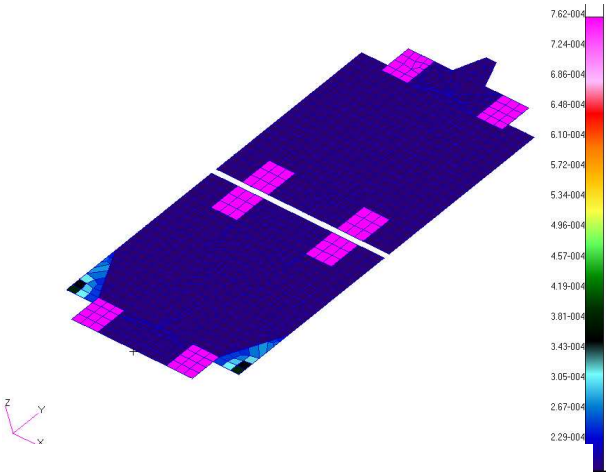

Figure 8. MGS example: thickness definition on hot side facesheet (m).

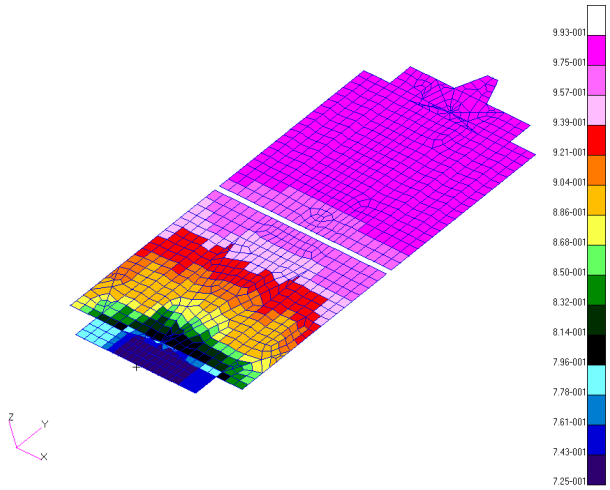

Figure 9. MGS viewfactors to space from solar cell side.

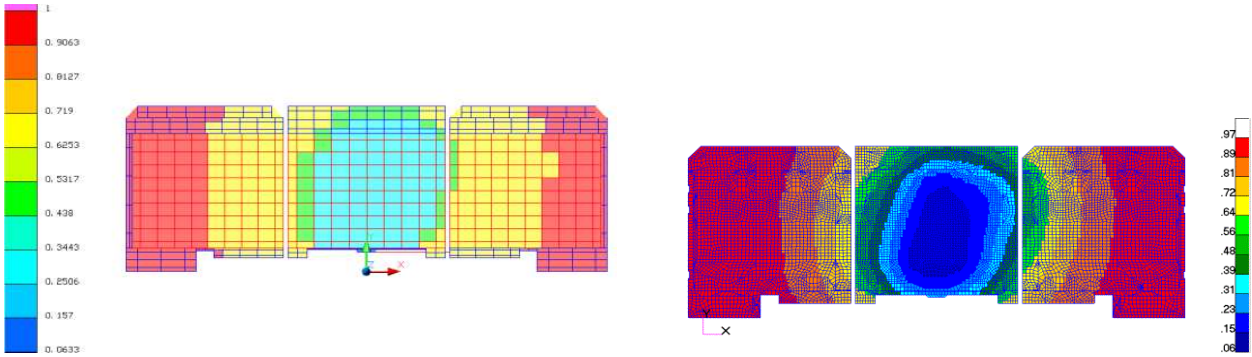

(a) (b)

Figure 10. Odyssey view factors to space: (a) Thermal Desktop, (b) mapped to PATRAN.

The aeroheating flux array was a function of both physical position on the array, and time within the drag pass. The aeroheating was interpolated in both time and space onto the PATRAN model on the entire exterior. User-developed FORTRAN was used within PATRAN to accomplish this interpolation. Example heating maps at a single time point are shown in Figure 11 for MGS and Figure 12 for Odyssey. On MGS, the inboard corners of the array received the highest heating, which was the reason for localized use of white paint and thickened Kapton.

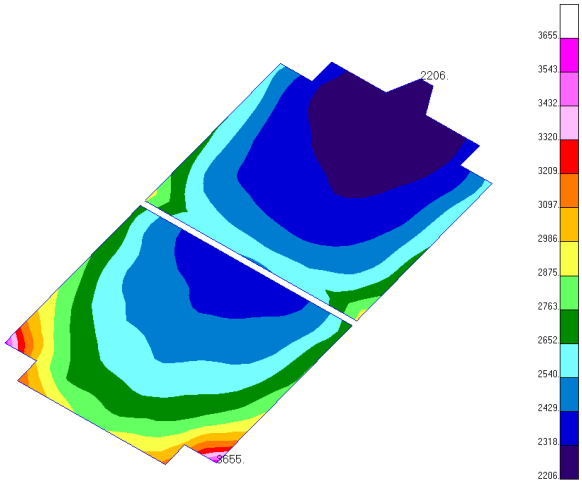

Figure 11. Example of MGS aeroheating mapped to the PATRAN model (W/m^2).

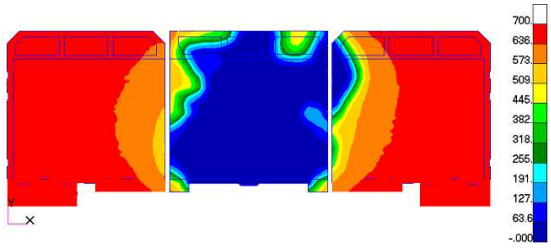

Figure 12. Example of Odyssey aerodynamic heating mapped to the PATRAN model (W/m2).

THERMAL RESULTS

The initial thermal runs for both missions showed differences from flight data, which were corrected through the process of correlating the model. The initial thermal results for both missions, and the correlation process, are described in detail elsewhere[9,10].

For MGS, the final corrected run to the pass 15 flight data is shown in Figure 13. The solid lines are flight data, and the lines with data markers are model predictions. The hottest thermocouple is predicted very well, and all others are conservative (i.e., prediction is somewhat too warm). Another interesting comparison was the difference between the hot side and cell side sensors, both on the outboard and inboard panels. This illustrates the model accuracy in both through thickness and lateral conduction, since the sensors were separated not only by the thickness of the panel, but also by most of the area of the panel as well. The hot side to cell side differences for MGS are shown in Figure 14.

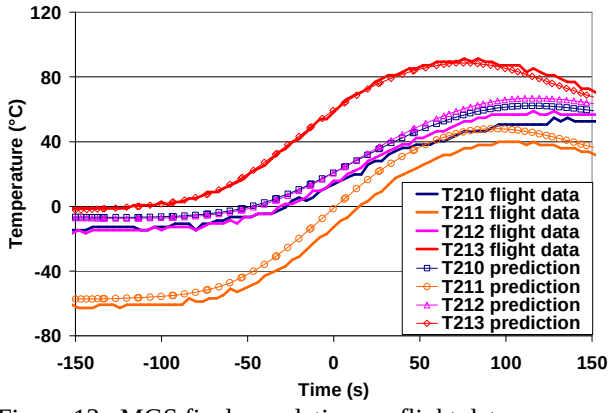

Figure 13. MGS final correlation vs. flight data.

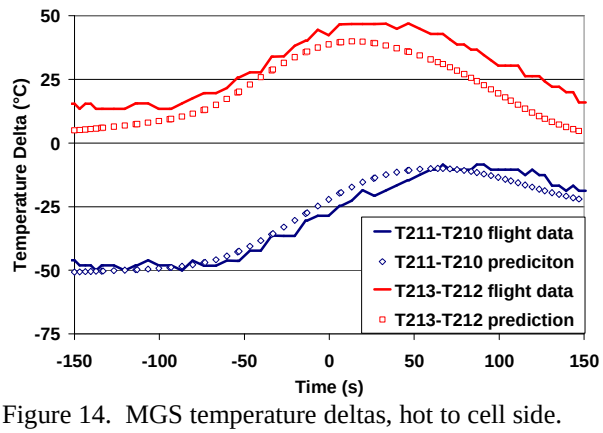

Figure 14. MGS temperature deltas, hot to cell side.

Overall quality of the MGS model correlation was evaluated in several ways, which are listed in Table 1. The primary measure of correlation was the change in temperature due to aerobraking. This difference in peak temperature change between model and flight, regardless of the timing, is shown in the row "Difference in peak temperature change". The worst value on a sensor was 4.4°C. Another measure was the time difference between when peak temperature was reached between the model and flight, shown in the row "Difference in peak timing". The difference in actual peak temperature is listed next in the table; differences of about 8°C reflect the inaccuracy of the starting temperatures. The RMS difference in the aeroheating temperature rise was calculated, which gives a measure of the accuracy of the model over all times, not just at the peak. The worst RMS difference was 6.7°C. The largest overall difference between prediction and flight over all time points was worst for T211 at 12°C. The final row gives the error of the model as a percentage, based on the first row values (peak temperature rise). If the RMS of these is taken, it gives an overall correlation error of 3%. All these measures point to a robust model that reflects in-flight performance accurately. After this correlation, two other earlier passes were selected at random to run and compare with flight data, and these yielded similar correlation quality measures.

Table 1. Correlation Quality Measures for MGS

	T210	T211	T212	T213
Difference in peak temperature change (°C)	-0.7	4.4	-1.6	-1.8
Difference in peak timing (sec)	-12.7	-0.7	-0.7	-0.7
Difference in peak actual temperature	7.5	8.0	8.0	-2.8
RMS difference in temperature change over time (°C)	2.6	6.7	2.1	2.9
Largest difference by time point (°C)	5.5	12.0	4.4	6.2
Difference in peak temperature change (%)	-1%	4%	-2%	-2%

The 3D thermal maps of the MGS correlated model are also useful to visualize the overall thermal condition of the array. In all of these figures, the thickness dimension is exaggerated to improve visualization. The initial predicted temperature gradient prior to the start of aerobraking is shown in Figure 15. The white painted areas are shown to be effective in cooling the inboard corners of the array, which are expected to receive the highest aeroheating fluxes. The prediction at the time of peak temperature is shown in Figure 16. The inboard corners have been effectively pre-cooled, so that they do not become the hottest parts of the array. The mass of the hinges can be shown to locally slow down temperature rise. The effects of the relatively high conductance along the facesheets, and lower conductance through the core, can be seen.

A benefit of the full 3D model is that the maximum temperature prediction for each component or material can be calculated and compared with its maximum service temperature. Since MGS had already undergone aeroheating at the time of this modeling, this capability was not of use to this program, but in general this information can be used in the design process as well as in the trajectory planning. An example is shown in Figure 17. All materials remained well within their service limits, as expected since the aeroheating levels actually experienced were much less than the design target.

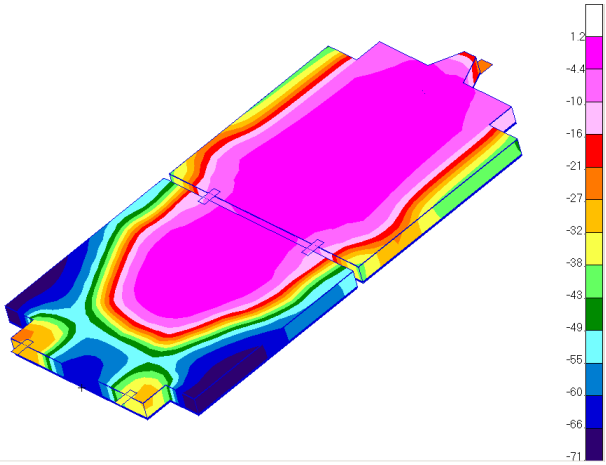

Figure 15. MGS thermal map prior to aerobraking (°C).

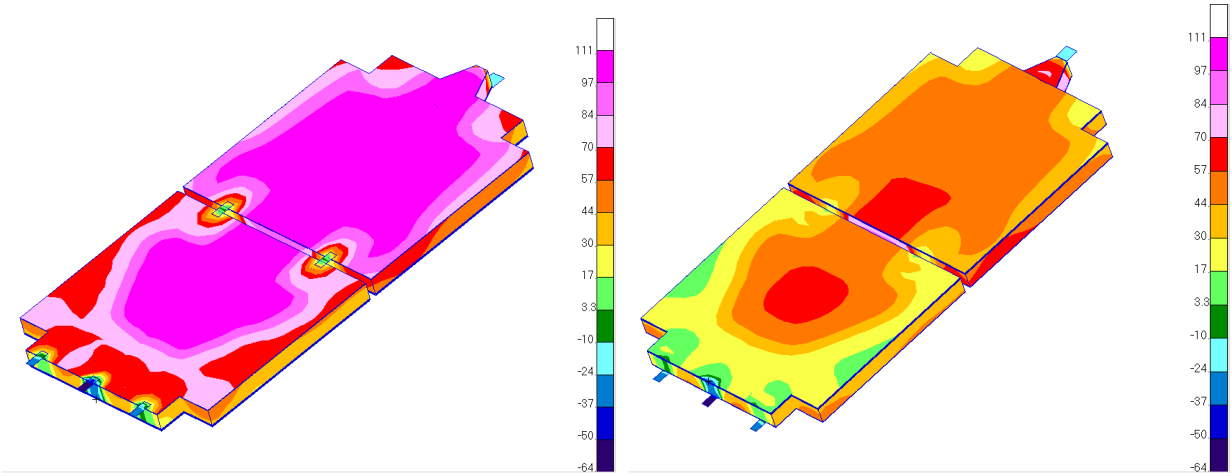

(a) hot side (b) cell side

Figure 16. MGS thermal map at 70 sec (near peak temperature) (°C).

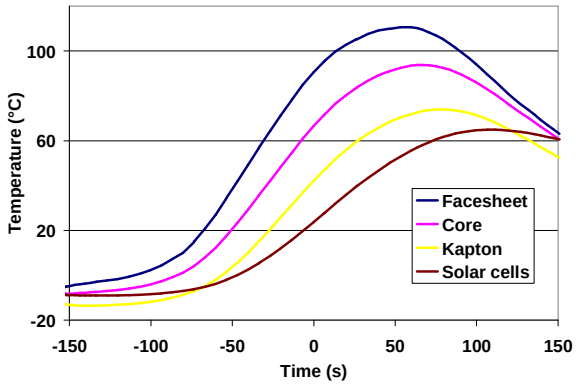

Figure 17. MGS material maximum predictions.

The Mars Odyssey correlation benefited from all the lessons learned on MGS, and also utilized flight data from orbit maneuvers enroute to Mars to improve correlation prior to aerobraking. After aerobraking started, additional adjustments were made to improve correlation. Figure 18 shows orbit pass 106 with all of the correlation adjustments applied. The mid panel thermocouple, T3, matches the flight data exactly. The difference between the facesheet thermocouples (T1 & T4) and the flight data was reduced to less than 10°C for the duration of the drag pass. There is still some overshoot error between the cell side thermocouples, T2 and T5. T3 matching the flight data as well as it does is an indication that overall, the through panel conductance was correlated very well.

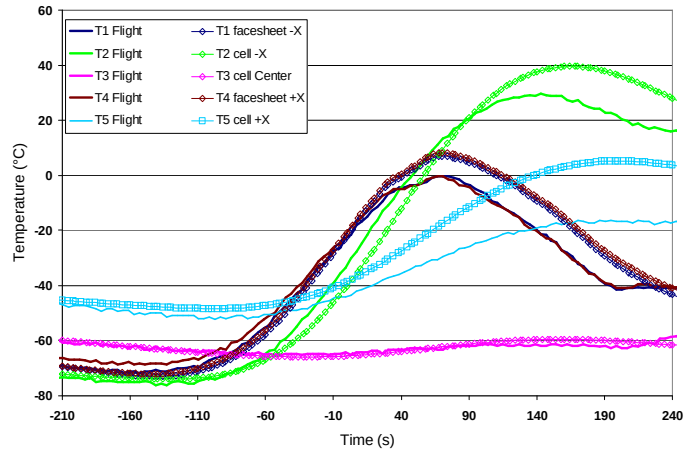

Figure 18. Odyssey reconstructed temperatures, orbit pass 106, using the best correlated thermal model.

The difference between flight and prediction for the cell side thermocouples T2 and T5 may be explained by the local conductance at those locations. The solar cell side was modeled as a single, continuous layer of material. In reality, the solar array has wires, solder, and some spots where there are no solar cells. The thermocouples T2 and T5 are in regions without solar cells, so they are mounted directly to the Kapton layer. Locally, there is less mass, and most significantly, lower solar absorptivity. Lower solar absorptivity in these local regions would reduce the amount of solar and planetary heat flux and thus reduce the temperature in these regions as observed in the flight data. The difference in local absorptivity was not modeled, but for future missions certainly should be.

As mentioned previously, Odyssey encountered the highest density of the mission on orbit pass 106, and hence this was the orbit pass with the largest aerodynamic heat flux. The higher heat flux intensified the effect of not including the local differences in solar heat flux. Looking at only orbit 106 can be deceiving because the differences between the flight data and the thermal model are maximized – in general, the differences throughout the mission were not this great.
Table 2 summarizes the average differences in peak temperatures for each thermocouple at three different points during the main phase of aerobraking and gives the overall mission average.
Table 2 shows that for the most part, the thermal model matched the peak flight thermocouple temperatures quite well – usually within 3°C. The peak temperature is the most critical, since those are the values used to set the drag pass heating flux levels.

Table 2. Summary of Peak Temperature Differences between Odyssey Flight Data and Thermal Model

	Average Peak Temperature Difference (°C)			
Sensor	Orbits 005 - 019	Orbits 020 - 095	Orbits 096 - 225	Mission Average
T1	4.1	3.1	2.1	2.90
T2	3.2	1.7	4.6	2.97
T3	0.1	0.2	0.2	0.16
T4	3.8	3.6	3.3	3.47
T5	6.5	6.9	9.2	7.53

Taking a closer look at the temperatures over the entire drag pass, a root mean squared (RMS) average for each thermocouple over the duration of the drag pass was computed. Table 3 shows the RMS average for each thermocouple at three points during the main phase of aerobraking. The RMS average provides a somewhat better means with which to assess how close the model was coming to the flight data for the duration of each drag pass and also gives some insight into the progression of the correlation over the mission. This view of the entire transient shows that the thermal model still matches the flight data extremely well, albeit not as well as only comparing the peak temperatures. Combining all of the thermocouples into one average, the average difference in the peak temperatures over the entire mission was 3.4°C. The average RMS temperature difference over the entire mission was 5.0°C.

Table 3. Summary of RMS Temperature Differences between Odyssey Flight Data and Thermal Model

	RMS Temperature Difference (°C)			
Sensor	Orbits 005 - 019	Orbits 020 - 095	Orbits 096 - 225	Mission Average
T1	7.2	6.2	4.3	5.90
T2	4.6	4.1	5.4	4.70
T3	2.0	3.1	1.9	2.33
T4	6.9	6.5	5.6	6.33
T5	3.9	3.7	5.7	4.43

Figure 19 shows the predicted temperature distribution on the Odyssey arrays for orbit pass 40, just after periapsis, which is typical of the majority of the drag passes encountered. This temperature distribution was calculated using a predicted density, and velocity profile, and assumed a nominal orientation relative to the atmosphere. A transient plot was generated for each material, where the maximum predicted temperature for any location on that material is tracked. Figure 20 shows the maximum material temperatures as a function of time.

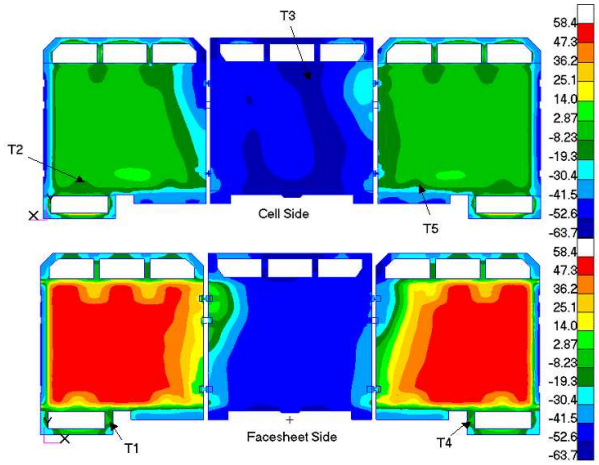

Figure 19. Odyssey predicted temperature distribution on the solar array for orbit pass 40 (°C).

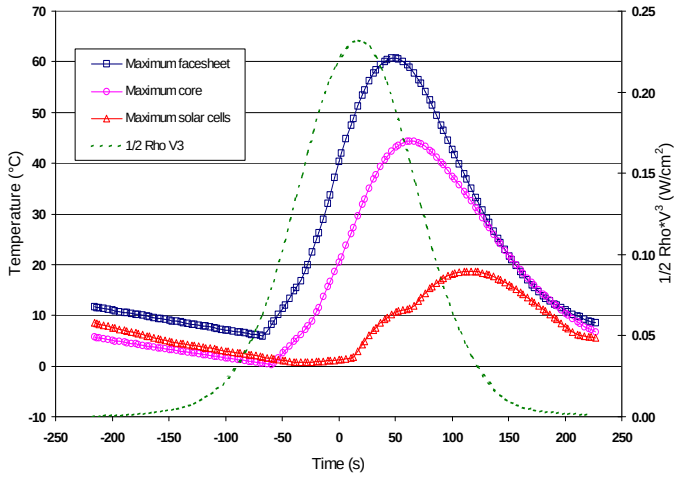

Figure 20. Odyssey maximum predicted material temperatures, orbit pass 040, peak heat flux = 0.232 W/cm2.

IMPROVEMENTS TO THE METHODOLOGY

Two improvements have recently been made to these methods: consolidating the orbital heating process to allow multiple configurations in a single run, and simplifying the aeroheating interpolation process.

During these modeling efforts, it was evident that accurate prediction of the initial temperatures was extremely important in predicting the actual peak temperature in the solar array. The Odyssey model used in operations included a prediction of the initial temperatures, but it was not coupled to the temperature predictions for each drag pass. The initial temperatures were determined when the spacecraft was in the vacuum phase and in its transition to the aerobraking configuration. Solutions for the view factors and orbital heating rates were obtained at several locations in the vacuum phase. In particular, solutions were obtained when the spacecraft was in its vacuum phase configuration (Figure 7), after the solar array was in its stowed position, after the spacecraft slewed into the aerobraking configuration (Figure 3), after the spacecraft passed into the eclipse region, and finally just prior to the start of the drag pass. Using PATRAN, and starting with a steady state solution for the temperatures with the spacecraft in the vacuum phase configuration, separate transient solutions had to be made between each of the above orbit event segments. Each transient solution used the prior solution's final set of temperatures as their starting temperatures. The temperatures had to be calculated in this fashion because the original methodology could only incorporate one solution for view factors and orbital heating for any one single transient. During the drag pass, the view factors were constant and the orbital heating changed very little across the array, which made this implementation acceptable. For each transient, the view factors and orbital heating field within PATRAN had to be modified and a new set of analysis files had to be generated from within PATRAN. This modification process was time prohibitive and therefore

could not be performed for every orbit pass during operations. The initial temperature prediction was updated on a weekly basis using the median orbit pass for that week. This simplification, along with breaking the orbit up into separate transients, introduced inaccuracies in the initial temperature prediction. To couple the initial temperature prediction to each drag pass and have it run as one transient requires some additional capability be incorporated into the user developed FORTRAN routine. Thermal Desktop has the ability to output a text file that contains the node locations, along with the currently posted data set. Text output can be generated for every orbit position, for both the view factors and the orbital heating, thus giving view factors and orbital heating as a function of time. The FORTRAN was then modified to read these output files and perform a time interpolation, as well as a spatial interpolation between the Thermal Desktop mesh and the PATRAN mesh. Since both Thermal Desktop and the drag pass trajectory information referenced periapsis as time zero, it was a simple matter to adjust the time scale and have the transient start at the desired point in the orbit in the vacuum phase and run through the completion of the drag pass. Including the orbital heating as a function of time is straightforward and application to the PATRAN model is identical to the method for aerodynamic heating. Including the view factors as a function of time requires changing the way radiation to space is calculated. Normally, the user specifies a radiation boundary condition within PATRAN as just that. PATRAN then builds a radiation network using the applied nodal subareas, the user-supplied view factors, and surface emissivity. In the case of the current methodology, the view factors were supplied as a finite element (FEM) field. To include these variable view factors, the radiation to space had to be applied as a heat flux boundary condition; making this heat flux negative produced the desired result of energy leaving the surface. To make the radiation calculation, the user FORTRAN was modified to include a radiative heat flux calculation using the classic radiation heat transfer equation.

The second improvement was to eliminate the Matlab script used to process the DSMC aerodynamic heating data, and the trajectory data. Originally, the Matlab script had to be run for every orbit pass, taking as input the current orbits atmospheric density and relative velocity as a function of time. The script then performed a data mining function to extract the heat transfer coefficient (C_H) from the DSMC database and make the heating calculation given by equation 1. The script then wrote out files that included the time, the DSMC grid X,Y,Z location and the heating value at that location. This was done to make use of the user FORTRAN that already existed to read and apply heating data in this format. This method produces inefficiencies in the code since for every time step, and for every node that has aerodynamic heating, a bivariate spatial interpolation and an interpolation over time had to be made. Significant improvement can be made by mapping the DSMC data to the PATRAN mesh prior to any PATRAN run, in effect building a DSMC database that is referenced to the PATRAN mesh. This was accomplished by using a Tecplot macro that performed a spatial interpolation of the DSMC data onto the PATRAN mesh. This produced a text file for every density that contained the PATRAN node number along with the interpolated C_H value. The user FORTRAN was modified to read these files, read the time dependant trajectory data, and make the heat flux calculation using equation 1. Then for every time step, and every node that has aerodynamic heating, the procedure is reduced to an interpolation over time to obtain the density, and an interpolation over density to get the C_H value. Both of these improvements were implemented and tested using Odyssey data, and produced temperatures that were within 0.1°C of the original runs. These improvements have been incorporated into the thermal model for the Mars Reconnaissance Orbiter, the next spacecraft planning to aerobrake around Mars.

CONCLUSIONS

Full 3D thermal models of the solar arrays for both MGS and Mars Odyssey were developed. Innovative methods were developed to integrate the true orbital heating, including shadowing, as well as aerobraking heating into the solar array thermal model. Thermal predictions at sensor locations were compared to the flight data and good correlation was obtained. Measures of correlation quality were differences in peak prediction to flight peak, as well as the RMS difference. Using these, model accuracy was in the range 3 to 6%. Use of a fully physical correlated thermal model was important for several reasons. Correlating the thermal model gave an overall snapshot of the entire aerobraking analysis process and how well each of the different disciplines' analysis models were performing. Also, the entire thermal behavior of the array can be visualized, and maximum temperature predictions can be obtained for each material. More accurate thermal predictions allows more accurate setting of the thermal limit lines that determine the depth of each aerobraking pass, which can substantially improve the time required to achieve orbit, as well as the final orbit attained. Improvements were made after these modeling efforts, which further streamlined the process. For example, initial temperature was predicted more accurately by incorporating several vacuum phase configuration changes into a single transient thermal run.

ACKNOWLEDGEMENTS

The authors would like to thank Michael Griffin and Richard Kriegbaum at Lockheed Martin Astronautics for providing drawings, details of the assemblies, and advice. Thanks are due to the entire Mars Odyssey flight operations team at Langley, in particular Richard Wilmoth for help with the aeroheating calculations, Dick Powell for his support, and Bob Tolson for initiating this effort. Also, thanks go out to the JPL navigation team for giving us the opportunity to make a contribution to this mission. We would also like to thank Mike Lindell for providing supporting structural analysis.

ACRONYMS

DSMC	Direct Simulation Monte Carlo
MGS	Mars Global Surveyor
MLI	Multilayer insulation
RMS	Root-mean-square

REFERENCES

[1] Carpenter, A. S., "The Magellan Aerobraking Experiment: Attitude Control Simulation and Preliminary Flight Results", AIAA Paper 93-3830, August 1993.

[2] Neuman, J. C., Buescher, J. A., and Esterl, G. J., "Magellan Spacecraft Thermal Control System Design and Performance", AIAA 28th Thermophysics Conference, Orlando, Florida, AIAA 93-2844, July 6-9, 1993.

[3] Haas, B. L., Feiereisen, W. J., "Particle Simulation of Rarefied Aeropass Maneuvers of the Magellan Spacecraft", AIAA 27th Thermophysics Conference, Nashville, Tennessee, AIAA 92-2923, July 6-8, 1992.

[4] Haas, B. L., Schmitt, D. A., "Simulated Rarefied Aerodynamics of the Magellan Spacecraft During Aerobraking", AIAA 93-3676-CP, July 6-9, 1993.

[5] Engineering Drawings from Lockheed Martin (919M0000020), SpectroLab Inc. (041312-041314), and Spectrum Astro Inc. (AM 111372-001, -002, -003) Various release dates 1997-1998.

[6] Dec, John A., and Amundsen, Ruth M., "A Thermal Analysis Approach for the Mars Odyssey Spacecraft's Solar Array", AIAA 2003 Thermophysics Conference, Orlando, Florida, June 2003.

[7] Thermal Desktop user manual, Cullimore and Ring Technologies, Inc., Version 3.2, August 2000.

[8] MSC/PATRAN User Manual, MacNeal-Schwendler Corporation, Version 2000 (r2), August 2000.

[9] Amundsen, Ruth M., Dec, John A., and George, Benjamin, E. LT., "Aeroheating Thermal Model Correlation for Mars Global Surveyor (MGS) Solar Array", AIAA 2003 Thermophysics Conference, Orlando, Florida, June 2003.

[10] Dec, John A., Gasbarre, Joseph, and George, Benjamin, E. LT., "Thermal Analysis and Correlation of the Mars Odyssey Spacecraft's Solar Array During Aerobraking Operations", AIAA 2002 Astrodynamics Conference, Monterey, California, AIAA 2002-4536, August 2002.